Inorganic Chemistry

pubs.acs.org/IC

Article

Exploration of the Structural and Vibrational Properties of the Ternary Molybdate $Tl_5BiHf(MoO_4)_6$ with Isolated MoO_4 Units and Tl^+ Conductivity

Victoria Grossman, Sergey V. Adichtchev, Victor V. Atuchin,* Bair G. Bazarov, Jibzema G. Bazarova, Natalia Kuratieva, Aleksandr S. Oreshonkov, Natalia V. Pervukhina, and Nikolay V. Surovtsev

Cite This: *Inorg. Chem.* 2020, 59, 12681−12689

Read Online

ACCESS | Metrics & More | Article Recommendations | Supporting Information

ABSTRACT: The phase relations in the subsolidus region of the Tl_2MoO_4−$Bi_2(MoO_4)_3$−$Hf(MoO_4)_2$ system were studied with the "intersecting cuts" method. The formation of the novel ternary molybdate $Tl_5BiHf(MoO_4)_6$ is found in this ternary system. The compound has a phase transition at T_{pt} = 731 K (ΔH = −3.15 J/g) and melts at T_m = 871 K (ΔH = −41.71 J/g), as determined by a thermal analysis. $Tl_5BiHf(MoO_4)_6$ single crystals were obtained by the spontaneous nucleation method. The crystal structure of $Tl_5BiHf(MoO_4)_6$ was revealed by structure analysis methods. This molybdate crystallizes in the trigonal space group $R\bar{3}c$ with the unit cell parameters a = 10.6801(4) Å, c = 38.5518(14) Å, V = 3808.3(2) Å^3, and Z = 6. The vibrational characteristics of $Tl_5BiHf(MoO_4)_6$ were determined by Raman spectroscopy. The $Tl_5BiHf(MoO_4)_6$ conductivity was measured at frequencies of 0.1, 1.0, and 10 kHz in the temperature range of 293−773 K; in this temperature range, the conductivity level was 10^{-12}−10^{-7} S/cm.

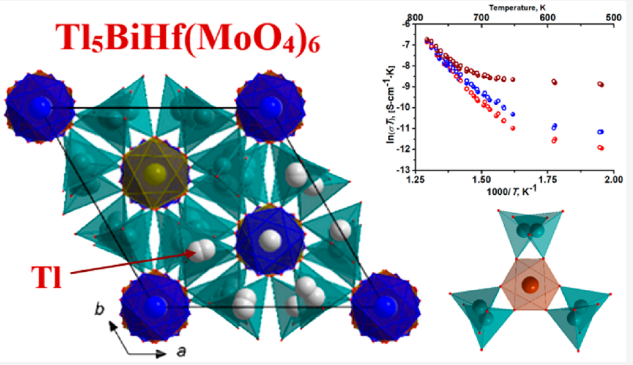

1. INTRODUCTION

Molybdate crystals have interesting optical, magnetic, electrical, and microstructural properties, and therefore, they are promising for such applications as laser and phosphor materials, microwave devices, scintillation materials, sensors, and catalysts.[1−7] In oxide crystals, in most cases, the Mo^{6+} ion is coordinated by six or four O^{2-} ions, and the resulting molybdenum coordination polyhedra can be significantly distorted. The specific features of the molybdate structures provide a diverse crystal chemistry of molybdate crystals and create a high feasibility for the incorporation of different metals into the basic family generating structures.[8−14]

Bismuth-containing oxide compounds have been reported as superconductors ($Bi_4V_2O_{11}$),[15,16] antiferromagnetic (Bi_2CuO_4)[17,18] and nonlinear optical materials,[19−21] and catalysts.[22,23] It was established that the presence of Bi^{3+} ions leads to a distortion of crystal structure due to the electrostatic effect. The compounds generated by combining Bi^{3+} cations with such tetrahedral anions as MoO_4, WO_4, VO_4, and PO_4 are among the promising functional materials, especially as laser hosts. Several binary molybdates containing monovalent metals and bismuth, such as $TBi(MoO_4)_2$ (T = Li−Cs, Ag) and $T_5Bi(MoO_4)_4$ (T = K, Cs, Tl), belong to ferroelectrics and ferroelastics,[24] solid electrolytes,[25,26] optical materials,[27] and phosphors.[28]

In recent years, ternary molybdates containing two different cations, Bi^{3+} ions and anionic groups MoO_4^{2-}, have been extensively studied. The phase equilibria and properties of compounds formed in several such systems were evaluated. Thus, in Li_2MoO_4−T_2MoO_4−$Bi_2(MoO_4)_3$ systems, the $LiTBi_2(MoO_4)_4$ (T = K, Tl, Rb) compounds isostructural with $BaLn_2(MoO_4)_4$ crystallized in the $C2/c$ space group[29,30] were detected. The formation of $NaCs_2Bi(MoO_4)_3$ and $Na_{7.72}Cs_{11}Bi_{3.76}(MoO_4)_{15}$[31−33] was found in the Na_2MoO_4−Cs_2MoO_4−$Bi_2(MoO_4)_3$ system, while $Cs_5BiA(MoO_4)_6$ and $Cs_2BiA_2(MoO_4)_{6.5}$ molybdates were obtained in the systems Cs_2MoO_4−$Bi_2(MoO_4)_3$−$A(MoO_4)_2$ (A = Zr, Hf).[34,35] $Cs_5BiA(MoO_4)_6$ ternary molybdates are considered as prospective materials for cesium immobilization from the waste of nuclear technologies.[35] However, in crystal chemistry, a certain similarity is known in the ionic radii of Cs^+ and Tl^+ cations[36] and, respectively, a similarity in the phase formation can be reasonably assumed for T_2MoO_4−$Bi_2(MoO_4)_3$−

Received: June 15, 2020
Published: August 12, 2020

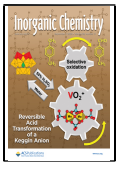

$A(MoO_4)_2$ (T = Cs, Tl; A = Zr, Hf) systems. In this relation, the present work is aimed at the observation of the formation of ternary Tl-containing bismuth molybdates in the system Tl_2MoO_4–$Bi_2(MoO_4)_3$–$Hf(MoO_4)_2$.

2. EXPERIMENTAL SECTION

The complex molybdate compositions in the system Tl_2MoO_4–$Bi_2(MoO_4)_3$–$Hf(MoO_4)_2$ were prepared by the solid-state reaction method. Tl_2O_3 (chemically pure, Red Chemist, Russia), Bi_2O_3 (chemically pure, Ural Plant of Chemical Reagents, Russia), HfO_2 (chemically pure, IGIC RAS, Russia), and MoO_3 (chemically pure, Red Chemist, Russia) were used as the starting reagents. It should be pointed out that Tl_2O_3 is a quite toxic oxide. Thus, for safety, when working with thallium-containing compounds, one should follow the needed precautions, including protective clothing, hand gloves, and respirator. The ternary compositions were prepared via a two-step synthesis route with the use of simple molybdates as intermediate materials. As was previously shown, this protocol is optimal to avoid MoO_3 loss during high-temperature annealing and was successfully realized in the preparation of several binary and ternary molybdates.[37−41] First, the elemental oxides were weighed in the stoichiometric ratios and the simple molybdates Tl_2MoO_4, $Bi_2(MoO_4)_3$, and $Hf(MoO_4)_2$ were synthesized by solid state reactions at 673−823, 723−773, and 673−1023 K, respectively. Then, these simple molybdates were used in the powder form as starting reagents in the preparation of ternary compositions and single-crystal growth.

Differential scanning calorimetry (DSC) was carried out with an NETZSCH STA 449 F1 TG/DSC/DTA (Jupiter) thermal analyzer. The sample charge was 18 mg, and the rate of temperature rise was 10 K/min under the Ar atmosphere. The differential thermal analysis (DTA) curves were calculated using a specially developed program from Netzsch.

The single-crystal X-ray diffraction data for $Tl_5BiHf(MoO_4)_6$ (**I**) were collected on a Bruker Apex DUO CCD diffractometer equipped with graphite-monochromated Mo Kα (λ = 0.71073 Å) radiation at 298(2) K. The ω-scan technique was employed to measure intensities. The absorption corrections were applied empirically using the SADABS program.[42] The structure was solved by the direct methods of a difference Fourier synthesis and further refined by the full-matrix least-squares method using the SHELXTL package.[43] The atomic thermal parameters for all atoms were refined anisotropically. The centrosymmetric space group $R\bar{3}c$ was chosen by proceeding from an analysis of the absences in the intensity array supported by calculations. The structure refinement shows the cooperative occupation of Bi and Hf atom positions. The self-occupancy factors (SOF) for Bi and Hf atoms in positions M(1) and M(2) were refined from the difference electron density maps and fixed at a ratio of 0.92/0.08 for M(1) (opposite for M(2)) in the final refinement to reduce the shifts. The position of Tl1 is split with the occupation (about 89%) mostly in the site of Tl1A.

The powder X-ray diffraction measurements were performed on a Bruker D8 ADVANCE diffractometer (Cu Kα, Vantec-1, maximum angle 2θ = 100°, scan step 0.01−0.02°). An X-ray phase analysis was carried out at room temperature and normal atmospheric pressure for all samples. To identify the powder sample phase composition, the obtained XRD pattern was compared with the theoretical diffraction pattern calculated on the basis of the structure data obtained for $Tl_5BiHf(MoO_4)_6$ by the single-crystal structure analysis.

The Raman experiment was carried out at room temperature in the backscattering geometry without polarization selection by using a Millennia solid-state laser (Spectra Physics) with wavelength 532.1 nm and Trivista 777 triple-grating Raman spectrometer. The spectral resolution of the spectrometer was ~1 cm^{-1}, and the incident laser beam intensity was about 60 mW. A neon-discharge lamp was used for the wavelength calibration of the spectrometer.

The electric conductivity with heating and cooling of the samples in the temperature range of 293−773 K was measured using a two-contact impedance spectroscopy method in the frequency range of 1−10^6 Hz (impedance meter "Z-1500J"). The samples were tablets, pressed by a PLG-12 hydraulic laboratory press, with platinum electrodes.

3. RESULTS AND DISCUSSION

3.1. Ternary System Tl_2MoO_4–$Bi_2(MoO_4)_3$–$Hf(MoO_4)_2$.

In the Tl_2MoO_4–$Bi_2(MoO_4)_3$–$Hf(MoO_4)_2$ system, the phase formation was explored by the method of "intersecting cuts" in the subsolidus region.[44,45] The data on the boundary binaries of the Tl_2MoO_4–$Bi_2(MoO_4)_3$–$Hf(MoO_4)_2$ concentration triangle were found in the literature and verified experimentally. In the binary systems Tl_2MoO_4–$Bi_2(MoO_4)_3$[46] and Tl_2MoO_4–$Hf(MoO_4)_2$,[47] the double molybdates $TlBi(MoO_4)_2$, $Tl_5Bi(MoO_4)_4$, $Tl_8Hf(MoO_4)_6$, and $Tl_2Hf(MoO_4)_3$ were previously found. The system $Bi_2(MoO_4)_3$–$Hf(MoO_4)_2$ is non phase forming.[48] The phase-pure compounds from the pointed boundary systems were initially synthesized, and these compounds were used as starting reagents for the preparation of ternary samples. The compositions corresponding to the points where the ternary system binary sections meet were prepared in two ways: from constituent simple molybdates or from double molybdates that belong to boundary binary systems.

An XRD phase analysis was carried out for the samples corresponding to the intersection points of the joins linking the points of the components and boundary compounds. This opens the possibility of finding the quasi-binary joins and performing the system triangulation. To prepare the samples of selected composition, a stoichiometric mixture of the molybdates was thoroughly ground with the use of an agate mortar. The powder samples were annealed at 723−823 K for 100−150 h in the air. The powder sample of $Tl_5BiHf(MoO_4)_6$ molybdate was synthesized by the solid-state reaction method. The stoichiometric mixture of simple molybdates Tl_2MoO_4, $Bi_2(MoO_4)_3$, and $Hf(MoO_4)_2$ was treated at 723 K for 24 h and at 773 K for 72 h in the air with intermittent grinding every 24 h in an agate mortar for sample homogenization. The synthesized product was white.

The phase equilibria of the Tl_2MoO_4–$Bi_2(MoO_4)_3$–$Hf(MoO_4)_2$ system in the subsolidus region are shown in Figure 1. The joins $Tl_5Bi(MoO_4)_4$–$Tl_8Hf(MoO_4)_6$, $TlBi(MoO_4)_2$–$Tl_8Hf(MoO_4)_6$, $TlBi(MoO_4)_2$–$Tl_2Hf(MoO_4)_3$, $TlBi(MoO_4)_2$–$Hf(MoO_4)_2$, $TlBi(MoO_4)_2$–$Tl_5BiHf(MoO_4)_6$, $Tl_5BiHf(MoO_4)_6$–$Tl_8Hf(MoO_4)_6$, and $Tl_5BiHf(MoO_4)_6$–

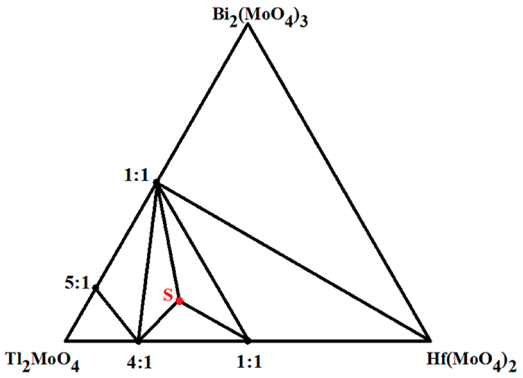

Figure 1. Phase equilibria of the Tl_2MoO_4–$Bi_2(MoO_4)_3$–$Hf(MoO_4)_2$ system in the subsolidus region of 723−823 K, where point S is related to $Tl_5BiHf(MoO_4)_6$.

https://dx.doi.org/10.1021/acs.inorgchem.0c01762
Inorg. Chem. 2020, 59, 12681−12689

$Tl_2Hf(MoO_4)_3$ divide the Tl_2MoO_4–$Bi_2(MoO_4)_3$–$Hf(MoO_4)_2$ system into seven subsystems.

Previously, the triple molybdates of composition $T_5BiA(MoO_4)_6$ were formed in T_2MoO_4–$Bi_2(MoO_4)_3$–$A(MoO_4)_2$ (T = K, Rb, Cs; A = Hf, Zr) systems.[35,49−51] There are no published data on lithium- or sodium-containing systems. The subsolidus structures of potassium and thallium systems are similar. The rubidium and cesium systems are distinguished by the fact that, along with the formation of ternary molybdates $T_5BiA(MoO_4)_6$ (T = Rb, Cs; A = Hf, Zr), molybdates $T_2BiHf_2(MoO_4)_{6.5}$ (T = Rb, Cs; A = Hf, Zr) are formed. An analysis of the experimental results reveals the decisive influence of dimensional factors on the formation of molybdates $T_2BiA_2(MoO_4)_{6.5}$.

The results of combined TG/DSC analysis of a $Tl_5BiHf(MoO_4)_6$ powder sample over the temperature range of 310−900 K are shown in Figure 2. The DSC heating curve clearly

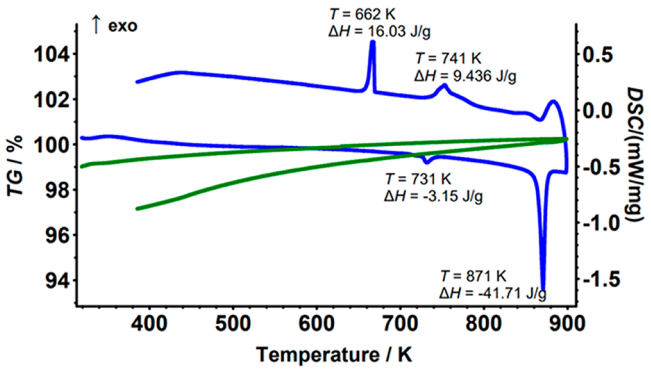

Figure 2. DSC/TG (blue/green) curves obtained on the $Tl_5BiHf(MoO_4)_6$ powder.

shows the endothermic effects attributed to the first-order phase transition at T_{pt} = 731 K (ΔH = −3.15 J/g) and incongruent melting of the $Tl_5BiHf(MoO_4)_6$ molybdate at T_m = 871 K (ΔH = −41.71 J/g). On the DSC curve related to cooling, two exo effects at 741 K (ΔH = 9.436 J/g) and 662 K (ΔH = 16.03 J/g) were detected and they were related to the crystallization of the compounds appeared due to the $Tl_5BiHf(MoO_4)_6$ decomposition. The TG curves recorded in the heating (green curve above) and cooling (green curve below) cycles are well reproducible, and there is no weight loss. This clearly indicates the absence of volatile components in the sample.

It is interesting to compare the thermal parameters determined for $Tl_5BiHf(MoO_4)_6$ with those of the compounds $T_5LA(MoO_4)_6$ (T = K, Rb, Cs, Tl; L = In, Bi, Ln; A = Zr, Hf), whose thermal properties were previously measured. The available thermal parameters are given in Table 1.[41,52−55] As is evident, first-order phase transitions were detected in all known $M_5LA(MoO_4)_6$ crystals, except for $K_5ScHf(MoO_4)_6$, and the structural transition in the temperature range of T_{pt} = 731−910 K is a specific effect of the compounds in this crystal family. The highest value of T_{pt} = 910 K is observed in $K_5InHf(MoO_4)_6$, and other known values are in the relatively narrow range of T_{pt} = 731−821 K. Thus, it appears that the T_m value is less sensitive to the type of T^+ and A^{4+} cations, and particularly high T_{pt} values can be predicted for $M_5InA(MoO_4)_6$ compounds. A similar relation is observed for the T_m values, and especially high T_m values can be assumed for In-containing compounds.

Table 1. Thermal Properties of the Compounds $T_5LA(MoO_4)_6$ (T = K, Rb, Cs, Tl; L = In, Sc, Bi, Ln; A = Zr, Hf)

compound	T_{pt}, K	T_m, K	ΔH_{pt}, J/g	ΔH_m, J/g	ref
$K_5DyZr(MoO_4)_6$	778	893			52
$K_5HoZr(MoO_4)_6$	777	913			52
$K_5YZr(MoO_4)_6$	769	927			52
$K_5ErZr(MoO_4)_6$	770	929			52
$K_5TmZr(MoO_4)_6$	753	952			52
$K_5YbZr(MoO_4)_6$	752	969			52
$K_5LuZr(MoO_4)_6$	752	981			52
$K_5InHf(MoO_4)_6$	910	1015	−1.279	−44.48	53
$K_5ScHf(MoO_4)_6$		999			54
$Rb_5CeZr(MoO_4)_6$	760, 809	883			55
$Rb_5NdZr(MoO_4)_6$	742, 813	928			55
$Rb_5TbZr(MoO_4)_6$	735, 817	936			55
$Rb_5ErZr(MoO_4)_6$	821	952			55
$Tl_5HoZr(MoO_4)_6$	721,819	852			41
$Tl_5BiHf(MoO_4)_6$	731	871	−3.15	−41.71	this study

3.2. $Tl_5BiHf(MoO_4)_5$ Growth and Structure. Single crystals of $Tl_5BiHf(MoO_4)_6$ were grown by crystallization in a solution-melt during a spontaneous nucleation. The previously synthesized molybdate $Tl_5BiHf(MoO_4)_6$ was used as a flux. A eutectic mixture containing molybdenum oxide and thallium molybdate (38 mol % of MoO_3 and 62 mol % of Tl_2MoO_4) was used as a solvent. The flux/solvent ratio in the prepared charge was equal to 1/3 (weight ratio). Initially, the charge was melted and kept at T = 823 K during 5 h for homogenization, and then the temperature was slowly decreased to T = 473 K at a cooling rate of 2 K/h. Then, the oven was turned off and the sample was cooled naturally to room temperature. The grown crystals were ∼1−2 mm in size. They were mechanically separated from the solid solvent cake by breaking up the ceramic crucible. For the structural analysis, the small perfect single crystals were selected with the use of an optical microscope. The structural quality of the selected crystals was further checked by the X-ray structural analysis.

The fragment of the $Tl_5BiHf(MoO_4)_6$ structure is displayed in Figure 3. The main crystallographic parameters and refinement details are presented in Table 2. The selected bond lengths in the $Tl_5BiHf(MoO_4)_6$ structure are given in Table 3. CCDC 2009239 contains the crystallographic data determined for the $Tl_5BiHf(MoO_4)_6$ compound. See the details on obtaining the file in Accession Codes.

The compounds $Tl_5BiHf(MoO_4)_6$, $Cs_5BiZr(MoO_4)_6$,[35] $K_5InHf(MoO_4)_6$,[56] and $Rb_5ErHf(MoO_4)_6$[57] are isostructural. The molybdenum atom is located in the general position in the structure. It is characterized by a tetrahedral oxygen coordination environment with a range of Mo−O bond lengths of 1.719(8)−1.820(6) Å and an average of 1.77(4) Å. This value is in agreement with the common Mo−O bond distance.[36] The variations in these distances, arising from different coordination types of O atoms to Tl, Bi, and Hf cations, are commensurate with the distances observed in other structures of similar composition and type.[35,56−59] The statistical distribution of $A^{2+}(A^{3+})$ and $Hf^{4+}(Bi^{3+})$ atoms over two crystallographic positions, M(1) and M(2), respectively, is a characteristic structural feature of this structural type.[32,53,54] This distribution of Bi/Hf atoms in positions M(1) and M(2) is in agreement with the M−O distances (Table 2). Position

https://dx.doi.org/10.1021/acs.inorgchem.0c01762
Inorg. Chem. 2020, 59, 12681−12689

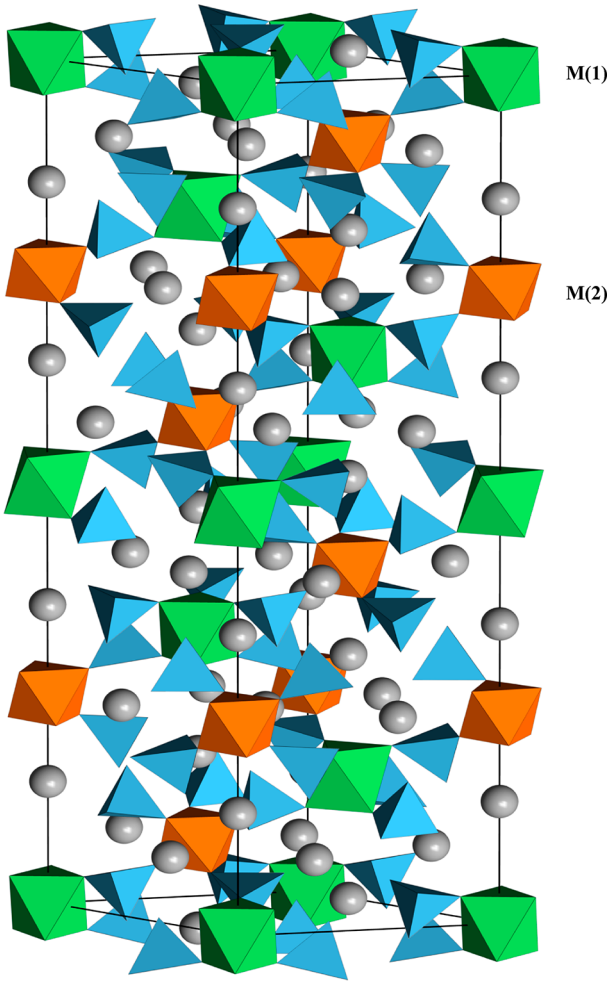

Figure 3. Crystal structure of $Tl_5BiHf(MoO_4)_6$. The unit cell is outlined. For clarity, the lone atoms are omitted. Tl atoms are shown as gray spheres.

M(1) coincides with the special point on axis $\bar{3}$, while position M(2) has a symmetry of 32, where axes 2 and 3 meet. The alkali-like thallium cations reside inside large polyhedra. The Tl1 atom position is split (positions Tl1A and Tl1B in the ratio 0.91/0.09). Both split positions lie on the 3-fold axis inside the polyhedron with nine tops with the triads of Tl1A−O distances equal to 2.859(7), 2.958(10), and 3.308(6) Å. The coordination polyhedron around a Tl2 atom, which is positioned on axis 2, is built by three pairs of closer O atoms (Tl2−O = 2.912(7)−3.148(6) Å) and three pairs of distant O atoms (Tl2−O = 3.331(8)−3.444(9) Å); this $Tl_5BiHf(MoO_4)_6$ array of O atoms forms the distorted-cuboctahedral environment. The crystal structure of $Tl_5BiHf(MoO_4)_6$ is a three-dimensional mixed-metal framework, which is built by a regular alternation of Mo tetrahedra and two types of $(Bi,Hf)O_6$ octahedra linked to one another via O-corner sharing (Figure 3). Large interstices of the framework, analogous to the frameworks considered in refs 35 and 56−59, accommodate two sorts of thallium cations.

It is interesting to consider the field of structural parameters available for $T_5LA(MoO_4)_6$ crystal family compounds. All of the $T_5LA(MoO_4)_6$ compounds whose unit cell parameters were reported are given in Table 4 and shown in Figure 4. As is evident from Table 4, a giant cell volume variation, by ∼13%, is possible in the $T_5LA(MoO_4)_6$ crystal family, and this indicates the high stability of this structure. As can be seen in Figure 4, on the $a-c$ plane, all known crystals can be covered by a narrow elongated inclined ellipse, whose ends are defined by $Cs_5BiZr(MoO_4)_6$ and ($K_5InHf(MoO_4)_6$, $K_5ScHf(MoO_4)_6$) points. The ellipse thickness is governed by $Rb_5CeZr(MoO_4)_6$ and $Ti_5BiHf(MoO_4)_6$. The relatively stable c/a ratio is a characteristic feature of the $T_5LA(MoO_4)_6$ crystal family and, in the design of new compounds, the selection of T−A cation pairs should be carried out by keeping $c/a \approx 3.5-3.6$.

The XRD pattern measured for the synthesized powder sample of $Tl_5BiHf(MoO_4)_6$ is presented in Figure 5. All of the peaks are successfully related to the $Tl_5BiHf(MoO_4)_6$ structure that verifies the powder sample phase purity. This powder sample was used in the following measurements of physical properties.

3.3. Vibrational Properties. The Raman spectrum of the powder $Tl_5BiHf(MoO_4)_6$ sample is displayed in Figure 6. As can be observed in Figure 3 and Table 3, the molybdenum atoms are coordinated by four oxygen atoms and they form the tetrahedral MoO_4^{2-} ions, which occupy the C_1 sites in the

Table 2. Crystal Data and Structure Refinement Details for $Tl_5BiHf(MoO_4)_6$

empirical formula	$BiHfMo_6O_{24}Tl_5$
formula wt	2368.96
cryst syst	trigonal
space group	$R\bar{3}c$
unit cell dimens	$a = b = 10.6801(4)$ Å
	$c = 38.5518(14)$ Å
V	3808.3(2) Å^3
Z	6
d_{calc}	6.198 g/cm^3
μ	45.514 mm^{-1}
$F(000)$	6024
cryst size	0.20 × 0.13 × 0.07 mm^3
θ range for data collection	2.44−30.52°
index ranges	$-11 \le h \le 15$
	$-15 \le k \le 14$
	$-51 \le l \le 54$
I_{hkl} coll	11438
I_{hkl} - $2\sigma_I$ (R_{int})	1293 (R_{int} = 0.0505)
completeness to θ = 25.25°	98.4%
max, min transmission	0.1428, 0.0397
no. of data/restraints/params	1293/0/61
goodness of fit on F^2	1.036
R ($I > 2\sigma_I$)	R1 = 0.0331, wR2 = 0.0873
R (I_{hkl} coll)	R1 = 0.0373, wR2 = 0.0892
extinction coeff	0.00024(2)
largest diff peak, hole	3.131, −95.112 e/Å^3

Table 3. Selected Interatomic Distances (d) for $Tl_5BiHf(MoO_4)_6$

Mo(1) tetrahedron		(Hf,Bi) octahedra	
bond	d, Å	bond	d, Å
Mo(1)−O(1)	1.786(7)	M(1)−O(1)	2.208(8) × 6
Mo(1)−O(2)	1.820(6)	M(2)−O(2)	2.054(5)−3.308(6) × 6
Mo(1)−O(3)	1.743(7)	Tl polyhedron	
Mo(1)−O(4)	1.719(8)	Tl(1A)−O	2.859(7)
⟨Mo(1)-O⟩	1.77(4)	Tl2 polyhedron	
		Tl(2)−O	2.912(7)−3.148(6)
			3.331(8)−3.444(9)

https://dx.doi.org/10.1021/acs.inorgchem.0c01762
Inorg. Chem. 2020, 59, 12681−12689

Table 4. Unit Cell Parameters of Ternary Molybdates $T_5LA(MoO_4)_6$ (T = K, Rb, Cs, Tl; L = In, Bi, Ln; A = Zr, Hf)

compound	$a = b$	c	V	Z	space group	ref
$K_5InHf(MoO_4)_6$	10.564(1)	37.632(4)	3637.0(6)	6	$R\bar{3}c$	56
$K_5LuHf(MoO_4)_6$	10.6536(1)	37.8434(8)	3719.75(9)	6	$R\bar{3}c$	60
$K_5ScHf(MoO_4)_6$	10.56312(8)	37.6251(3)	3635.74(6)	6	$R\bar{3}c$	54
$Tl_5BiHf(MoO_4)_6$	10.6801(4)	38.5518(14)	3808.3(2)	6	$R\bar{3}c$	this study
$Rb_5EuHf(MoO_4)_6$	10.7264(1)	38.6130(8)	3847.44(9)	6	$R\bar{3}c$	61
$Rb_5CeZr(MoO_4)_6$	10.7248(2)	38.796(1)	3864.52(14)	6	$R\bar{3}c$	58
$Rb_5ErHf(MoO_4)_6$	10.7511(1)	38.6543(7)	3869.31(9)	6	$R\bar{3}c$	57
$Rb_5NdZr(MoO_4)_6$	10.7561(2)	38.7790(12)	3885.41(16)	6	$R\bar{3}c$	59
$Rb_5NdHf(MoO_4)_6$	10.7550(2)	38.8427(13)	3891.0(2)	6	$R\bar{3}c$	62
$Cs_5BiZr(MoO_4)_6$	10.9569(2)	39.804(4)	4138.4(4)	6	$R\bar{3}c$	35

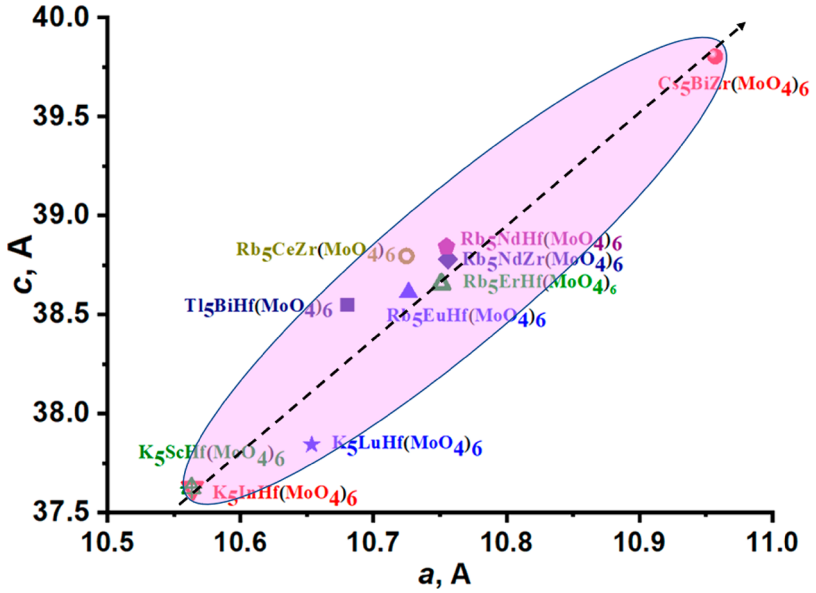

Figure 4. $T_5LA(MoO_4)_6$ (T = K, Rb, Cs, Tl; L = In, Bi, Ln; A = Zr, Hf) crystals on the $a-c$ plane.

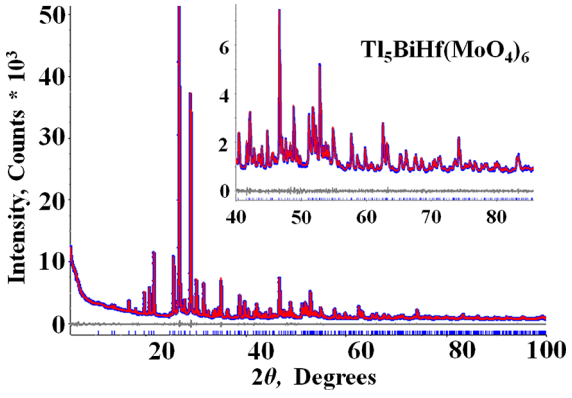

Figure 5. XRD pattern of the $Tl_5BiHf(MoO_4)_6$ powder sample.

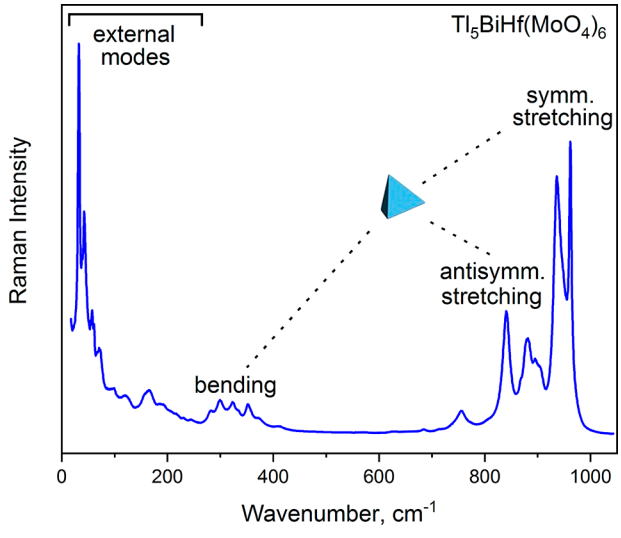

Figure 6. Raman spectrum of $Tl_5BiHf(MoO_4)_6$.

crystal structure. The internal vibrations of free MoO_4^{2-} tetrahedral ions can be denoted as ν_1 (A_1) symmetric and ν_3 (F_2) antisymmetric stretching modes and ν_2 (E) symmetric and ν_4 (F_2) antisymmetric bending modes. All of them are Raman-active. The modes ν_3 and ν_4 are infrared-active. The letters A, E, and F indicate nondegenerate and doubly and triply degenerate vibrations, respectively. The correlation between the MoO_4^{2-} ion (T_d symmetry), its site symmetry C_1, and factor group symmetry D_{3d} of the unit cell is shown in Table 5.[62]

As follows from the group theory, the vibrational representation at the Γ point of the Brillouin zone can be written as follows: $\Gamma_{vibr} = 18A_{1g} + 21A_{2g} + 39E_g + 20A_{1u} + 23A_{2u} + 43E_u$, where the acoustic modes are $A_{2u} + E_u$.[64] A_{1g} and E_g modes are active in Raman scattering, and A_{2u} and E_u modes are infrared-active. A_{2g} and A_{1u} modes are classified as

https://dx.doi.org/10.1021/acs.inorgchem.0c01762
Inorg. Chem. 2020, 59, 12681−12689

Table 5. Correlation Diagram for the MoO_4^{2-} Ion in $Tl_5BiHf(MoO_4)_6$

free ion symmetry		site symmetry		factor group symmetry
MoO_4^{2-}, T_d		C_1		D_{3d}
ν_1, A_1	→	A	→	$A_{1g} + A_{1u} + A_{2g} + A_{2u} + 2E_g + 2E_u$
ν_2, E	→	2A	→	$2A_{1g} + 2A_{1u} + 2A_{2g} + 2A_{2u} + 4E_g + 4E_u$
ν_3, ν_4, F_2	→	3A	→	$3A_{1g} + 3A_{1u} + 3A_{2g} + 3A_{2u} + 6E_g + 6E_u$
transl F_2		3A	→	$3A_{1g} + 3A_{1u} + 3A_{2g} + 3A_{2u} + 6E_g + 6E_u$
rot F_1		3A	→	$3A_{1g} + 3A_{1u} + 3A_{2g} + 3A_{2u} + 6E_g + 6E_u$

silent. According to the relations given in Table 5, one can expect the appearance of 12 spectral bands in the range of MoO_4 tetrahedral stretching vibrations: $A_{1g} + 2E_g$ (ν_1) and $3A_{1g} + 6E_g$ (ν_3). The deconvolution of the experimental spectrum (Figure S1) in the wavenumber range of 730−1010 cm^{-1} reveals at least 10 Raman modes. To match the Raman lines with irreducible representations, we need polarization-selective Raman spectra.[65] However, this is impossible in the case of a powder sample. In addition, spectral bands overlap in the Raman spectra with polarization selection. The observed strong bands above 900 cm^{-1} are attributed to symmetric stretching of the MoO_4 tetrahedra, and the remaining bands in the high-wavenumber region are antisymmetric stretching. The bands related to the ν_2 and ν_4 bending modes of the MoO_4 units are observed in the range of 260−430 cm^{-1} (Figure S2), and they can be listed as $2A_{1g} + 4E_g$ (ν_2) and $3A_{1g} + 6E_g$ (ν_4). The vibrations over the wavenumber range of 340−430 cm^{-1} are classified as the ν_4 modes, and those appeared at the wavenumbers between 260 and 340 cm^{-1} are related to the ν_2 modes.[66−68] The external modes consist of the translational vibrations of the Tl, Bi, Hf, and MoO_4^{2-} ions and MoO_4^{2-} librations[63] (Figure S3).

3.4. Electrical Properties. For the electrical measurements, disk-shaped tablets 10 mm in diameter and 2 mm in thickness were fabricated from the $Tl_5BiHf(MoO_4)_6$ powder at a pressure of 10 MPa. These tablets were treated at 723 K for 2 h and then cooled to room temperature in a cooling oven. Then, platinum paste electrodes with an area of $S \approx 75$ mm^2 were deposited on the base surfaces of the ceramic disks. The electric conductivity σ at each temperature was obtained by the relation $\sigma = 4h/\pi D^2 R$, where h is the thickness of the sample, D is the tablet diameter, and R is the resistance.

The temperature dependences of conductivity at frequencies 0.1, 1, and 10 kHz are shown in Figure 7 as $\ln(\sigma T)$ versus reciprocal temperature. It is seen that the conductivity increases with temperature due to the increase in the free charge carrier concentration. In addition, the conductivity significantly increases with the frequency, which is due to relaxation processes occurring at higher frequencies. At high temperatures, the conductivity increase obeys the Arrhenius thermal activation law and does not depend significantly on frequency. Curves $\sigma = f(T)$ have anomalies related to the phase transition at 731 K. As can be seen in Figure 7, the curves recorded on heating and cooling modes coincide.

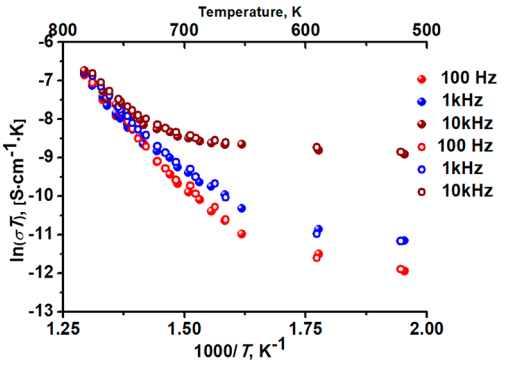

Figure 7. $Tl_5BiHf(MoO_4)_6$ conductivity dependence on temperature at measuring field frequencies of 0.1, 1.0, and 10 kHz. The heating and cooling cycles are shown by filled and empty circles, respectively.

The $Tl_5BiHf(MoO_4)_6$ conductivity at the frequencies of 0.1, 1.0, and 10 kHz was determined in the temperature range of 293−773 K. In this temperature range, the conductivity varies in the range of 10^{-12}−10^{-7} S/cm. At 770 K, the $Tl_5BiHf(MoO_4)_6$ conductivity is as low as 10^{-7} S/cm, which is significantly lower than the conductivity of the isostructural K-containing compounds $K_5LZr(MoO_4)_6$ (L = Al, Cr, Fe, In, Sc)[69] and $K_5InHf(MoO_4)_6$.[53] As can be assumed, the conductivity decrease in Tl-containing crystals is induced by Tl^+ ions with a larger radius in reference to that of the K^+ ion. If this relation is general for the $T_5LA(MoO_4)_6$ crystal family, the conductivity of Cs-containing molybdates should be even lower than that of Tl-containing crystals. The conductivities of Tl- and Rb-containing crystals should be similar.

4. CONCLUSIONS

The formation of the ternary molybdate $Tl_5BiHf(MoO_4)_6$ is found in the ternary system Tl_2MoO_4−$Bi_2(MoO_4)_3$−$Hf(MoO_4)_2$. This is the first Tl-containing crystal in the $T_5LA(MoO_4)_6$ (T = K, Rb, Cs, Tl; L = In, Sc, Bi, Ln; A = Zr, Hf) family. As was obtained by a comparative analysis of the structural parameters known for $T_5LA(MoO_4)_6$ compounds, this structure type is exceptionally stable and the unit cell volume can vary by ∼13% via an ion substitution without a structure disruption. In addition, the number of isostructural compounds $T_5LA(MoO_4)_6$, including $Tl_5BiHf(MoO_4)_6$ as an only known Tl-containing representative, opens a possibility for the discovery of new "structure−composition−property" relations. Following this idea, we can assume that this kind of structure is a suitable framework for ion substitution. Thus, $T_5LA(MoO_4)_6$ molybdates are promising hosts for the creation of a wide range of doped materials, including phosphors with activation by rare-earth ions. The Raman spectroscopy results indicate that the symmetry of the MoO_4 tetrahedra is reduced, which is in accordance with the XRD results.

■ ASSOCIATED CONTENT

Supporting Information

The Supporting Information is available free of charge at https://pubs.acs.org/doi/10.1021/acs.inorgchem.0c01762.

Decomposition of Raman spectra (PDF)

Accession Codes

CCDC 2009239 contains the supplementary crystallographic data for this paper. These data can be obtained free of charge

https://dx.doi.org/10.1021/acs.inorgchem.0c01762
Inorg. Chem. 2020, 59, 12681−12689

via www.ccdc.cam.ac.uk/data_request/cif, or by emailing data_request@ccdc.cam.ac.uk, or by contacting The Cambridge Crystallographic Data Centre, 12 Union Road, Cambridge CB2 1EZ, UK; fax: +44 1223 336033.

AUTHOR INFORMATION

Corresponding Author

Victor V. Atuchin − *Laboratory of Optical Materials and Structures, Institute of Semiconductor Physics, SB RAS, Novosibirsk 630090, Russia; Laboratory of Semiconductor and Dielectric Materials, Novosibirsk State University, Novosibirsk 630090, Russia; Research and Development Department, Kemerovo State University, Kemerovo 650000, Russia;* orcid.org/0000-0002-7424-5604; Phone: +7 (383) 3308889; Email: atuchin@isp.nsc.ru

Authors

Victoria Grossman − *Laboratory of Oxide Systems, Baikal Institute of Nature Management, SB RAS, Ulan-Ude 670047, Russia;* orcid.org/0000-0001-8192-9847

Sergey V. Adichtchev − *Laboratory of Condensed Matter Spectroscopy, Institute of Automation and Electrometry, SB RAS, Novosibirsk 630090, Russia*

Bair G. Bazarov − *Laboratory of Oxide Systems, Baikal Institute of Nature Management, SB RAS, Ulan-Ude 670047, Russia; Buryat State University, Ulan-Ude 670000, Russia*

Jibzema G. Bazarova − *Laboratory of Oxide Systems, Baikal Institute of Nature Management, SB RAS, Ulan-Ude 670047, Russia*

Natalia Kuratieva − *Laboratory of Crystal Chemistry, Institute of Inorganic Chemistry, SB RAS, Novosibirsk 630090, Russia; Laboratory for Research Methods in Composition and Structure of Functional Materials, Novosibirsk State University, Novosibirsk 630090, Russia*

Aleksandr S. Oreshonkov − *Laboratory of Molecular Spectroscopy, Kirensky Institute of Physics Federal Research Center KSC SB RAS, Krasnoyarsk 660036, Russia; Siberian Federal University, Krasnoyarsk 660079, Russia;* orcid.org/0000-0003-3046-7018

Natalia V. Pervukhina − *Laboratory of Semiconductor and Dielectric Materials, Novosibirsk State University, Novosibirsk 630090, Russia; Laboratory of Crystal Chemistry, Institute of Inorganic Chemistry, SB RAS, Novosibirsk 630090, Russia*

Nikolay V. Surovtsev − *Laboratory of Condensed Matter Spectroscopy, Institute of Automation and Electrometry, SB RAS, Novosibirsk 630090, Russia;* orcid.org/0000-0002-1580-0508

Complete contact information is available at: https://pubs.acs.org/10.1021/acs.inorgchem.0c01762

Notes

The authors declare no competing financial interest.

ACKNOWLEDGMENTS

This study was supported by the Russian Science Foundation (19-42-02003, in the part of conceptualization). The study was also funded by the RFBR according to research projects 18-08-00985, 18-08-00799, and 18-03-00557. This study was carried out within the state assignment of the FASO of Russia (Theme No. 0339-2016-0007).

REFERENCES

(1) Basiev, T. T.; Sobol, A. A.; Voronko, Yu.K.; Zverev, P. G. Spontaneous Raman spectroscopy of tungstate and molybdate crystals for Raman lasers. *Opt. Mater.* **2000**, *15*, 205−216.

(2) Kuang, W.; Fan, Y.; Chen, Y. Structure and reactivity of ultrafine Fe-Mo oxide particles prepared by the sol-gel method. *Langmuir* **2000**, *16*, 5205−5208.

(3) Kersen, Ü.; Holappa, L. Surface characterization and H_2S-sensing potential of iron molybdate particles produced by supercritical solvothermal method and subsequent oxidation. *Appl. Phys. A: Mater. Sci. Process.* **2006**, *85*, 431−436.

(4) Paul, T.; Ghosh, A. Structure and vibrational properties of $La_{2-x}Bi_xMo_2O_9$ ($0.05 \leq x \leq 60.4$) oxygen ion conductors. *J. Alloys Compd.* **2014**, *613*, 146−152.

(5) Garcia-Cortes, A.; Serrano, M. D.; Zaldo, C.; Cascales, C.; Strömqvist, G.; Pasiskevicius, V. Nonlinear refractive indices of disordered $NaT(XO_4)_2$ T = Y, La, Gd, Lu and Bi, X = Mo, W femtosecond laser crystals. *Appl. Phys. B: Lasers Opt.* **2008**, *91*, 507−510.

(6) Shi, P.; Xia, Z.; Molokeev, M. S.; Atuchin, V. V. Crystal chemistry and luminescence properties of red-emitting $CsGd_{1-x}Eu_x(MoO_4)_2$ solid-solution phosphors. *Dalton Trans.* **2014**, *43*, 9669−9676.

(7) Lim, C. S.; Atuchin, V.; Aleksandrovsky, A.; Molokeev, M.; Oreshonkov, A. Microwave sol-gel synthesis of $CaGd_2(MoO_4)_4$:Er^{3+}/Yb^{3+} phosphors and their upconversion photoluminescence properties. *J. Am. Ceram. Soc.* **2015**, *98* (10), 3223−3230.

(8) Klevtsov, P. V.; Klevtsova, R. F. Polymorphism of the double molybdates and tungstates of mono- and trivalent metals with the composition $M^+R^{3+}(EO_4)_2$. *J. Struct. Chem.* **1977**, *18* (3), 419−439.

(9) Chimitova, O. D.; Atuchin, V. V.; Bazarov, B. G.; Molokeev, M. S.; Bazarova, Z. G. The formation and structural parameters of new double molybdates $RbLn(MoO_4)_2$ (Ln = Pr, Nd, Sm, Eu). *Proc. SPIE* **2013**, *8771*, 87711A.

(10) Grossman, V. G.; Bazarov, B. G.; Klevtsova, R. F.; Solodovnikov, S. F.; Glinskaya, L. A.; Fedorov, K. N.; Bazarova, Z. G. Phase equilibria in the Tl_2MoO_4-$Nd_2(MoO_4)_3$-$Hf(MoO_4)_2$ system and the crystal structure of double molybdate $TlNd(MoO_4)_2$. *Russ. J. Inorg. Chem.* **2008**, *53* (10), 1660−1665.

(11) Atuchin, V. V.; Bekenev, V. L.; Chimitova, O. D.; Molokeev, M. S.; Bazarov, B. G.; Bazarova, J. G.; Khyzhun, O. Y.; Lim, C. S. Synthesis and electronic properties of β-$RbNd(MoO_4)_2$. *Asian J. Chem.* **2014**, *26* (5), 1284−1286.

(12) Atuchin, V. V.; Khyzhun, O. Y.; Chimitova, O. D.; Molokeev, M. S.; Gavrilova, T. A.; Bazarov, B. G.; Bazarova, J. G. Electronic structure of V-$RbNd(MoO_4)_2$ by XPS and XES. *J. Phys. Chem. Solids* **2015**, *77*, 101−108.

(13) Lim, C. S.; Aleksandrovsky, A. S.; Molokeev, M. S.; Oreshonkov, A. S.; Ikonnikov, D. A.; Atuchin, V. V. Triple molybdate scheelite-type upconversion phosphor $NaCaLa(MoO_4)_3$:Er^{3+}/Yb^{3+}: structural and spectroscopic properties. *Dalton Trans.* **2016**, *45* (39), 15541−15551.

(14) Solodovnikov, S. F.; Atuchin, V. V.; Solodovnikova, Z. A.; Khyzhun, O. Y.; Danylenko, M. I.; Pishchur, D. P.; Plyusnin, P. E.; Pugachev, A. M.; Gavrilova, T. A.; Yelisseyev, A. P.; Reshak, A. H.; Alahmed, Z. A.; Habubi, N. F. Synthesis, structural, thermal, and electronic properties of palmierite-related double molybdate H-$Cs_2Pb(MoO_4)_2$. *Inorg. Chem.* **2017**, *56* (6), 3276−3286.

(15) Sammes, N. M.; Tompsett, G. A.; Näfe, H.; Aldinger, F. Bismuth based oxide electrolytes - structure and ionic conductivity. *J. Eur. Ceram. Soc.* **1999**, *19* (10), 1801−1826.

(16) Boivin, J. Electrode electrolyte BIMEVOX system for moderate temperature oxygen separation. *Solid State Ionics* **1998**, *113*−*115* (1−2), 639−651.

(17) Boivin, J. C.; Trehoux, J.; Thomas, D. Structural study of $CuBi_2O_4$. *Bull. Soc. Fr. Mineral Crystallogr.* **1976**, *99*, 193−195.

(18) Denisov, V. M.; Irtyugo, L. A.; Denisova, L. T.; Kirik, S. D.; Chumilina, L. G. High-temperature heat capacity of Bi_2CuO_4. *Phys. Solid State* **2012**, *54* (9), 1943−1945.

(19) Hellwig, H.; Liebertz, J.; Bohatý, L. Exceptional large nonlinear optical coefficients in the monoclinic bismuth borate BiB_3O_6 (BIBO). *Solid State Commun.* **1998**, *109* (4), 249−251.
(20) Lin, Z.; Wang, Z.; Chen, C.; Lee, M.-H. Mechanism for linear and nonlinear optical effects in monoclinic bismuth borate (BiB_3O_6) crystal. *J. Appl. Phys.* **2001**, *90* (11), 5585−5590.
(21) Mao, F.-F.; Hu, C.-L.; Xu, X.; Yan, D.; Yang, B.-P.; Mao, J.-G. $Bi(IO_3)F_2$: The first metal iodate fluoride with a very strong second harmonic generation effect. *Angew. Chem. - Int. Ed.* **2017**, *56* (8), 2151−2155.
(22) Xie, L.; Ma, J.; Xu, G. Preparation of a novel Bi_2MoO_6 flake-like nanophotocatalyst by molten salt method and evaluation for photocatalytic decomposition of rhodamine B. *Mater. Chem. Phys.* **2008**, *110*, 197−200.
(23) Liu, X.; Liu, Y.; Su, J.; Li, M.; Guo, L. Facile preparation of $BiVO_4$ nanoparticle film by electrostatic spray pyrolysis for photoelectrochemical water splitting. *Int. J. Hydrogen Energy* **2015**, *40* (38), 12964−12972.
(24) Isupov, V. A. Binary molybdates and tungstates of mono and trivalent elements as possible ferroelastics and ferroelectrics. *Ferroelectrics* **2005**, *321*, 63−90.
(25) Brilingas, A.; Grigas, I.; Gurskas, A.; Zvyagin, A. I.; Kalesinskas, V.; Pelikh, L. N. Dielectric properties of $CsBi(MoO_4)_2$ layered crystals on SHF. *Fizika Tverdogo Tela (in Russian)* **1980**, *22* (11), 3477−3479.
(26) Zhou, D.; Randall, C. A.; Pang, L.-X.; Wang, H.; Guo, J.; Zhang, G.-Q.; Wu, Y.; Guo, K.-T.; Shui, L.; Yao, X. Microwave dielectric properties of $(ABi)_{1/2}MoO_4$ (A = Li, Na, K, Rb, Ag) type ceramics with ultra-low firing temperatures. *Mater. Chem. Phys.* **2011**, *129* (3), 688−692.
(27) Hanuza, J.; Maczka, M. Vibrational properties of the double molybdates $MX(MoO_4)_2$ family (M = Li, Na, K, Cs; X = Bi, Cr): Part I. Structure and infrared and Raman spectra in the polycrystalline state. *Vib. Spectrosc.* **1994**, *7*, 85−96.
(28) Mazurak, Zb.; Blasse, G.; Liebertz, J. The Luminescence of the scheelite $NaBi(MoO_4)_2$. *J. Solid State Chem.* **1987**, *68* (1), 181−184.
(29) Khal'baeva, K. M.; Khaikina, E. G. Subsolidus structure of the Li_2MoO_4-Tl_2MoO_4-$Bi_2(MoO_4)_3$ system. *Russ. J. Inorg. Chem.* **2000**, *45* (2), 257−262.
(30) Klevtsova, R. F.; Glinskaya, L. A.; Alekseev, V. I.; Khalbaeva, K. M.; Khaikina, E. G. Crystal structural study of ternary molybdate $LiRbBi_2(MoO_4)_4$. *J. Struct. Chem.* **1994**, *34* (5), 789−793.
(31) Mokhosoev, M. V.; Kozhevnikova, N. M.; Khaikina, E. G.; Khazheeva, Z. I.; Alekseev, F. P.; Khal'baeva, K. M.; Basovich, O. M.; Nimaeva, E. N.; Abykova, E. R.; Tudupova, S. D. Triple molybdates of mono-, mono (bi)- and trivalent elements. *Abstracts of the VI All-Union Conference on the Chemistry and Technology of molybdenum and tungsten*, Nalchik, September 13−15, 1988; p 85.
(32) Savina, A. A. *Synthesis, structure and properties of new compounds in systems Na_2MoO_4-Cs_2MoO_4-$R_2(MoO_4)_3$ (R - trivalent metal)*, Ph.D. Thesis, Lomonosov Moscow State University, Moscow, 2013.
(33) Savina, A. A.; Atuchin, V. V.; Solodovnikov, S. F.; Solodovnikova, Z. A.; Krylov, A. S.; Maximovskiy, E. A.; Molokeev, M. S.; Oreshonkov, A. S.; Pugachev, A. M.; Khaikina, E. G. Synthesis, structural and spectroscopic properties of acentric triple molybdate $Cs_2NaBi(MoO_4)_3$. *J. Solid State Chem.* **2015**, *225*, 53−58.
(34) Bazarova, J. G.; Tushinova, Yu.L.; Bazarov, B. G.; Oyun, B. E.; Angarhayev, J. D. Phase equilibrium in the systems Cs_2MoO_4-$R_2(MoO_4)_3$-$Hf(MoO_4)_2$ (R = Al, Cr, Fe, Bi, La-Lu). *Izv. VUZov, Prikl. Khim. Biotekhnol.* **2018**, *8* (2), 19−28.
(35) Bazarov, B. G.; Namsaraeva, T. V.; Klevtsova, R. F.; Anshits, A. G.; Vereshchagina, T. A.; Kurbatov, R. V.; Glinskaya, L. A.; Fedorov, K. N.; Bazarova, Zh.G. Phase equilibrium in the Cs_2MoO_4-$Bi_2(MoO_4)_3$-$Zr(MoO_4)_2$ system and the crystal structure of new triple molybdate $Cs_5BiZr(MoO_4)_6$. *Russ. J. Inorg. Chem.* **2008**, *53* (9), 1484−1488.
(36) Shannon, R. D. Revised effective ionic radii and systematic studies of interatomic distances in halides and chalcogenides. *Acta Cryst. A* **1976**, *32*, 751−767.
(37) Grossman, V. G.; Bazarov, B. G.; Klevtsova, R. F.; Solodovnikov, S. F.; Glinskaya, L. A.; Fedorov, K. N.; Bazarova, Zh. G. Phase equilibria in the Tl_2MoO_4-$Nd_2(MoO_4)_3$-$Hf(MoO_4)_2$ system and the crystal structure of double molybdate $TlNd(MoO_4)_2$. *Russ. J. Inorg. Chem.* **2008**, *53* (10), 1660−1665.
(38) Atuchin, V. V.; Chimitova, O. D.; Gavrilova, T. A.; Molokeev, M. S.; Kim, S.-J.; Surovtsev, N. V.; Bazarov, B. G. Synthesis, structural and vibrational properties of microcrystalline $RbNd(MoO_4)_2$. *J. Cryst. Growth* **2011**, *318*, 683−686.
(39) Atuchin, V. V.; Grossman, V. G.; Adichtchev, S. V.; Surovtsev, N. V.; Gavrilova, T. A.; Bazarov, B. G. Structural and vibrational properties of microcrystalline $TlM(MoO_4)_2$ (*M* = Nd, Pr) molybdates. *Opt. Mater.* **2012**, *34* (5), 812−816.
(40) Atuchin, V. V.; Chimitova, O. D.; Adichtchev, S. V.; Bazarov, J. G.; Gavrilova, T. A.; Molokeev, M. S.; Surovtsev, N. V.; Bazarova, Zh.G. Synthesis, structural and vibrational properties of microcrystalline >-$RbSm(MoO_4)_2$. *Mater. Lett.* **2013**, *106*, 26−29.
(41) Grossman, V. G.; Bazarov, B. G.; Bazarova, Ts.T.; Glinskaya, L. A.; Bazarova, J. G.; Temuujin, J. Phase equilibria in the Tl_2MoO_4-$Ho_2(MoO_4)_3$-$Zr(MoO_4)_2$ system and the crystal structure of $Ho_2Zr_2(MoO_4)_7$ and $TlHoZr_{0.5}(MoO_4)_3$. *J. Ceram. Proc. Res.* **2017**, *18* (12), 875−881.
(42) *APEX2 (Ver. 1.08), SAINT (Ver. 7.03), and SADABS (Ver. 2.11)*; Bruker Advanced X-ray Solutions: Madison, Wisconsin, USA, 2004.
(43) Sheldrick, G. M. Crystal structure refinement with SHELXL. *Acta Crystallogr., Sect. C: Struct. Chem.* **2015**, *C71*, 3−8.
(44) Guertler, W. Z. Zur Fortentwicklung der Konstitutionsforschungen bei ternaren Systemen. *Anorg. Allg. Chem. Bd* **1926**, *154*, 439−455.
(45) Niepel, L.; Malinovsky, M. Triangulation of phase diagrams. *Chem. Zvesti* **1978**, *32*, 810−820.
(46) Khaikina, E. G. *Synthesis, phase formation and structures of binary and thernary molybdates of single- and trivalent metals*, D.Sc. thesis, Nikolaev Institute of Inorganic Chemistry, Novosibirsk, 2008.
(47) Bazarov, B. G.; Klevtsova, R.; Bazarova, Ts.T.; Glinskaya, L. A.; Fedorov, K. N.; Bazarova, Zh. G.; Chimitova, D. Systems Tl_2MoO_4-$E(MoO_4)_2$, where *E* = Zr or Hf, and the crystal structure of $Tl_8Hf(MoO_4)_6$. *Russ. J. Inorg. Chem.* **2006**, *51* (5), 794−799.
(48) Tushinova, Y. L.; Bazarova, J. G.; Arkhincheeva, S. I. Phase equilibriums in systems $R_2(MoO_4)_3$-$Zr(MoO_4)_2$, *Proc. of All-Russia Conf. Dedicated to Seventieth Anniv. of M.V. Mokhosoev*, June 27−30, 2002, Ulan-Ude, Russia; p. 90−91.
(49) Bazarova, J. G.; Tushinova, Y. L.; Logvinova, A. V.; Bazarov, B. G.; Dorzhieva, S. G.; Bazarova, T. T. Synthesis, structure and properties of triple molybdates of the $K_5RZr(MoO_4)_6$ composition in K_2MoO_4-$R_2(MoO_4)_3$-$Zr(MoO_4)_2$ systems (*R* = trivalent elements)), Izvestiya Vuzov. Prikladnaya Khimiya i Biotekhnologiya [Proceedings of Universities. *Izv. VUZov, Prikl. Khim. Biotekhnol.* **2019**, *9* (2), 202−211 (in Russian).
(50) Bazarova, T. T.; Chimitova, O. D.; Bazarov, B. G. Phase formation in Rb_2MoO_4-$R_2(MoO_4)_3$-$Hf(MoO_4)_2$ (*R* = Al, Cr, Fe, Sc, In, Y, Bi) systems. *Bull. Buryat State Univ.* **2012**, *3*, 21−23.
(51) Bazarova, J. G.; Tushinova, Yu.L.; Bazarov, B. G.; Oyun, B. E.; Angarhayev, J. D. Phase equilibrium in the systems Cs_2MoO_4-$R_2(MoO_4)_3$-$Hf(MoO_4)_2$ (*R* = Al, Cr, Fe, Bi, La-Lu), Izvestiya Vuzov. Prikladnaya Khimiya i Biotekhnologiya [Proceedings of Universities. *Izv. VUZov, Prikl. Khim. Biotekhnol.* **2018**, *8* (2), 19−28 (in Russian).
(52) Logvinova, A. V.; Bazarov, B. G.; Tushinova, Yu.L.; Bazarova, J. G. Phase relations in the K_2MoO_4-$Ln_2(MoO_4)_3$-$Zr(MoO_4)_2$ (*Ln* = La-Lu, Y) systems. *Inorg. Mater.* **2017**, *53* (12), 1286−1292.
(53) Grossman, V. G.; Bazarov, B. G.; Bazarova, J. G. $K_5InHf(MoO_4)_6$: A solid state conductor. *IOP Conf. Series: Earth and Environ. Sci.* **2019**, *320*, 012050.
(54) Grossman, V. G.; Bazarova, J. G.; Molokeev, M. S.; Bazarov, B. G. New triple molybdate $K_5ScHf(MoO_4)_6$: Synthesis, properties, structure and phase equilibria in the M_2MoO_4-$Sc_2(MoO_4)_3$-$Hf(MoO_4)_2$ (*M* = Li, K) systems. *J. Solid State Chem.* **2020**, *283*, 121143.

https://dx.doi.org/10.1021/acs.inorgchem.0c01762
Inorg. Chem. 2020, 59, 12681−12689

(55) Gongorova, L. I. *Phase equilibrium, structure and properties of new molybdates in the systems Rb_2MoO_4-$Ln_2(MoO_4)_3$-$Zr(MoO_4)_2$ (Ln = La-Lu)*, D.Sc. thesis, Irkutsk State University, Irkutsk, 2012.
(56) Bazarov, B. G.; Klevtsova, R. F.; Bazarova, Ts.T.; Glinskaya, L. A.; Fedorov, K. N.; Bazarova, Zh.G. Synthesis and crystal structure of triple molybdate $K_5InHf(MoO_4)_6$. *Russ. J. Inorg. Chem.* **2005**, *50* (8), 1146.
(57) Bazarov, B. G.; Klevtsova, R. F.; Chimitova, O. D.; Glinskaya, L. A.; Fedorov, K. N.; Tushinova, Yu.L.; Bazarova, Zh.G. Phase formation in the Rb_2MoO_4-$Er_2(MoO_4)_3$-$Hf(MoO_4)_2$ system and the crystal structure of new triple molybdate $Rb_5ErHf(MoO_4)_6$. *Russ. J. Inorg. Chem.* **2006**, *51* (5), 794.
(58) Gongorova, L. I.; Bazarov, B. G.; Chimitova, O. D.; Bazarova, Z. G.; Klevtsova, R. F.; Glinskaya, L. A.; Anshits, A. G.; Vereschagina, T. A. Crystal structure of a new ternary molybdate $Rb_5CeZr(MoO_4)_6$. *J. Struct. Chem.* **2012**, *53* (2), 329−333.
(59) Chimitova, O. D.; Bazarov, B. G.; Fedorov, K. N.; Dubentsov, A. V.; Gongorova, L. I.; Klevtsova, R. F.; Glinskaya, L. A.; Anshits, A. G. Crystal structure of triple molybdate in the Rb_2MoO_4-$Nd_2(MoO_4)_3$-$Zr(MoO_4)_2$ system. *J. Struct. Chem.* **2010**, *51* (1), 173−176.
(60) Romanova, E. Yu.; Bazarov, B. G.; Klevtsova, R. F.; Glinskaya, L. A.; Tushinova, Yu.L.; Fedorov, K. N.; Bazarova, Zh.G. Phase formation in the K_2MoO_4-$Lu_2(MoO_4)_3$-$Hf(MoO_4)_2$ system and the structural study of triple molybdate $K_5LuHf(MoO_4)_6$. *Russ. J. Inorg. Chem.* **2007**, *52* (5), 749−752.
(61) Bazarov, B. G.; Chimitova, O. D.; Klevtsova, R. F.; Tushinova, Yu.L.; Glinskaya, L. A.; Bazarova, Zh.G. Crystal structure of a new ternary molybdate in the Rb_2MoO_4-$Eu_2(MoO_4)_3$-$Hf(MoO_4)_2$ system. *J. Struct. Chem.* **2008**, *49* (1), 53−57.
(62) Chimitova, O. D.; Bazarov, B. G.; Klevtsova, R. F.; Fedorov, K. N.; Glinskaya, L. A.; Kuznetsov, M. V.; Bazarova, Z. G. Synthesis, crystal structure, and electrical properties of the new ternary molybdate $Rb_5NdHf(MoO_4)_{(6)}$. *Russ. Chem. Bull.* **2007**, *56* (11), 2135−2139.
(63) Nakamoto, K. *Infrared and Raman Spectra of Inorganic and Coordination Compounds*, 6th ed.; Wiley: New York, 2009.
(64) Smirnov, M. B.; Kazimirov, V. Yu. LADY: software for lattice dynamics simulations. *JINR communications* **2001**.E14-2001-159
(65) Peschanskii, A. V. Raman scattering study of the structural phase transition in single crystal $KDy(MoO_4)_2$. *Low Temp. Phys.* **2017**, *43*, 1315−1322.
(66) Lim, C. S.; Aleksandrovsky, A. S.; Molokeev, M. S.; Oreshonkov, A. S.; Atuchin, V. V. The modulated structure and frequency upconversion properties of $CaLa_2(MoO_4)_4$:Ho^{3+}/Yb^{3+} phosphors prepared by microwave synthesis. *Phys. Chem. Chem. Phys.* **2015**, *17*, 19278−19287.
(67) Lim, C. S.; Atuchin, V. V.; Aleksandrovsky, A. S.; Molokeev, M. S.; Oreshonkov, A. S. Incommensurately modulated structure and spectroscopic propertiesof $CaGd_2(MoO_4)_4$:Ho^{3+}/Yb^{3+} phosphors for up-conversion applications. *J. Alloys Compd.* **2017**, *695*, 737−746.
(68) Atuchin, V. V.; Aleksandrovsky, A. S.; Bazarov, B. G.; Bazarova, J. G.; Chimitova, O. D.; Denisenko, Y. G.; Gavrilova, T. A.; Krylov, A. S.; Maximovskiy, E. A.; Molokeev, M. S.; Oreshonkov, A. S.; Pugachev, A. M.; Surovtsev, N. V. Exploration of structural, vibrational and spectroscopic properties of self-activated orthorhombic double molybdate $RbEu(MoO_4)_2$ with isolated MoO_4 units. *J. Alloys Compd.* **2019**, *785*, 692−697.
(69) Bazarova, J. G.; Logvinova, A. V.; Bazarov, B. G.; Tushinova, Y. L.; Dorzhieva, S. G.; Temuujin, J. Synthesis of new triple molybdates $K_5RZr(MoO_4)_6$ (R = Al, Cr, Fe, In, Sc) in the K_2MoO_4-$R_2(MoO_4)_3$-$Zr(MoO_4)_2$ systems, their structure and electrical properties. *J. Alloys Compd.* **2018**, *741*, 834−839.

https://dx.doi.org/10.1021/acs.inorgchem.0c01762
Inorg. Chem. 2020, 59, 12681−12689